RSC Advances

This is an *Accepted Manuscript*, which has been through the Royal Society of Chemistry peer review process and has been accepted for publication.

Accepted Manuscripts are published online shortly after acceptance, before technical editing, formatting and proof reading. Using this free service, authors can make their results available to the community, in citable form, before we publish the edited article. This *Accepted Manuscript* will be replaced by the edited, formatted and paginated article as soon as this is available.

You can find more information about *Accepted Manuscripts* in the **Information for Authors**.

Please note that technical editing may introduce minor changes to the text and/or graphics, which may alter content. The journal's standard **Terms & Conditions** and the **Ethical guidelines** still apply. In no event shall the Royal Society of Chemistry be held responsible for any errors or omissions in this *Accepted Manuscript* or any consequences arising from the use of any information it contains.

ROYAL SOCIETY
OF CHEMISTRY

www.rsc.org/advances

Kinetics and mechanism for OH-initiated gas-phase chemistry of α-terpineol

Yan Zhao[a], Haitao Sun[b], Mei Qin[b], Renjun Wang[a], Laixiang Xu[*,a]

_____

[a] School of Life Sciences, Qufu Normal University, Qufu, 273165, P. R. China

[b] School of Chemistry and Chemical Engineering, Qufu Normal University,

Qufu, 273165, P. R. China

[*] Corresponding author. E-mail: xlx150723@163.com

Fax: 86-537-4456887

1

1

Abstract

3   *α*-Terpineol, mainly released from the widely used cleaning products, is an important

4   indoor air pollutant. In this paper, the OH-initiated degradation mechanism of *α*-terpineol was

5   studied by employing Density Functional Theory (DFT) method. The reaction scheme is

6   proposed for the initial steps. Two barrierless addition processes and the H7-abstraction from

7   the ring are found to be the main reaction pathways. The products, such as

8   6-hydroxy-hept-5-en-2-one, 4-oxopentanal, acetone, and 4-methyl-3-cyclohexen-1-one, have

9   been detected experimentally, which are confirmed by this theoretical investigation. The

10   suggested formation mechanism of 4-methyl-3-cyclohexen-1-one in the experimental study is

11   not energetically feasible; instead, here an energetically favorable pathway is reported for the

12   first time. The overall rate constant of the title reaction is evaluated to be 1.29×10^{-10} cm^3

13   molecule^{-1} s^{-1}. The gas-phase residential time of *α*-terpineol with the respect of OH is about

14   3.1 hours.

15

16

17

18

19

20

21

22

1. Introduction

Volatile organic compounds (VOCs) with a high vapor pressure, can be easily released into indoor air from various VOC emission sources, acting as the main air pollutants in the indoor environment.[1] Previous experimental results have showed that the VOC concentrations in indoors are 10 times higher than in outdoor environments.[2-5] Therefore, the influence of long-time exposure to indoor air contaminants on the health of human beings has attracted more and more attention. It has already been accepted that extensive exposure to VOCs can cause various acute and chronic health effects, such as acute and chronic respiratory effects, neurological toxicity (e.g., fatigue, headaches, etc.), eye and throat irritation, and even lung cancer.[5-11] Hence, the fate of VOCs in indoor environment is worth studying.

Terpenoids as common additives to numerous consumer products (perfumes, soaps, shampoos, deodorants, etc.) and meantime a kind of prevalent VOCs indoors, have received increasing attention .[12-16] Most of the terpenoids are reported to be present at significant indoor concentrations.[17,18] Among them, 1-Methyl-4-isopropyl-1-cyclohexen-8-ol (α-terpineol, **Scheme 1**) is the main component of indoor cleaner emissions and pine oil,[17] as well as an emission from some molds existing in the indoor environment.[19-21]

Once emitted into the indoor air, α-terpineol tends to undergo complex chemical transformations by O_3 , OH radicals, and NO_3 radicals existed in air,[22] generating various more irritating secondary pollutants (such as alcohols, aldehydes, ketones, dicarbonyls, carboxylic acids, and organic nitrates).[3] Based on the above, we can conclude that the gas-phase oxidation of α-terpineol has great influences on the indoor air quality, which should be systematically investigated. Unfortunately, little is known about the gas-phase chemistry of

1 α-terpineol. Jones and Ham have investigated the indoor reaction mechanism and the products

2 formed during the reaction between α-terpineol and NO_3 radicals. The rate constant of the

3 NO_3 radical with α-terpineol was measured by a relative rate method.[23] Wells, et al. have

4 studied the gas-phase oxidation of α-terpineol by OH radicals and O_3 in the presence of NOx

5 using smog chamber GC/MS techniques.[24] The rate constants were determined to be (1.9±

6 0.5)×10^{-10} and (3.0±0.2)×10^{-16} cm^3 molecule^{-1} s^{-1}，respectively. Several reaction products

7 were analyzed using the mass spectrometry. Nevertheless, the actual reaction pathways for the

8 observed products have been still unclear due to the lack of geometric parameters for

9 intermediate radical species. Direct experimental detection of the intermediate species is

10 extremely difficult because of their short lifetimes. Quantum chemical calculations have been

11 proven to be a promising way to determin the geometrical structures of the reactants,

12 intermediates, transition states and products created in the detailed reaction mechanism and to

13 investigate the kinetics property of the corresponding reaction system.[25-28]

14 Considering that there are currently no experimental or theoretical kinetic data on the

15 OH-initated reactions, here we performed a theoretical study on the OH-initiated gas-phase

16 oxidation reaction of α-terpineol in the indoor environment using density function theory

17 (DFT).[29] The rate constants were evaluated by employing the multichannel

18 Rice-Ramsperger-Kassel-Marcus (RRKM) theory to find out the rate controlling steps of the

19 distinct reaction pathways.

20 **2. Computational Methods**

21 The quantum chemical calculations were performed using the Gaussian 09 program

22 suite.[30] The MPWB1K function was employed to optimize the geometries of the reactants,

1   intermediates, transition states and products at the MPWB1K/6-31+G(d,p) level in this

2   paper.[31] It is well known that MPWB1K and BB1K methods give good results for barrier

3   height and reaction energy calculations with the mean unsigned errors of about 1 kcal

4   mol^{-1}.[31-33] The selection of the MPWB1K method for this work is detailed in the

5   Supplementary material. The harmonic vibrational frequency calculations at the same level

6   of theory were used to identify that whether the optimized structures are the true minima or

7   the transition state. For each transition state, the intrinsic reaction coordinate (IRC) was

8   calculated to determine the connections between the reactants, the transition states, and the

9   products.[34] To accurately obtain total electronic energies, additional single-point high-level

10   *ab* initio calculations were carried out at the MPWB1K/6-311+G(3df,2p) level of

11   computation upon MPWB1K/6-31+G(d,p) optimized structures. The potential energy

12   surface profile was conducted at the MPWB1K/6-311+G(3df,2p)//MPWB1K/6-31+G(d)

13   level including zero-point vibration energy (ZPVE) correction.

14   The kinetic calculations including tunneling corrections were carried out using

15   Rice−Ramsperger−Kassel−Marcus (RRKM) theory with the open source MESMER

16   program.[35,36] The reliability of the tunneling corrections is detailed in the Supplementary

17   material. This method has been successfully applied to several theoretical studies.[37,38]

18   The microcanonical rate constants were computed using the RRKM equation:

19
$$k(E) = \frac{W(E)}{h\rho(E)} \tag{1}$$

20   where, $W(E)$ is the rovibrational sum of states at the transition state, $\rho(E)$ is density of states

21   of reactants, and h is Planck's constant. Then, the canonical rate constant $k(T)$ is determined

22   from the following equation:

$$1 \qquad k(T) = \frac{1}{Q(T)} \int k(E) \rho(E) \exp(-\beta E) dE \qquad\qquad (2)$$

2   where, $Q(T)$ is the reactant partition function.

3. Results and discussion

4   The reliability of the calculated results in this study was validated first. The experimental

5   information on the thermochemical parameters for α-terpineol is not available and the direct

6   comparison between the theoretical calculations and the experimental data becomes

7   impossible. Hence, we performed the geometry optimization and frequency calculation of

8   cyclohexene and ethanol. The results at the MPWB1K/6-31+G(d,p) level agree fairly well

9   with the corresponding experimental values. The largest deviation remains within 1.8% for

10   geometrical parameters and 7.0% for vibrational frequencies.[39,40] Consequently, we believe

11   that the MPWB1K-DFT/6-31+G(d,p) method is a general and reliable method for the

12   calculations involved in the OH-initiated oxidation of α-terpineol.

3.1. Reaction mechanism

3.1.1. Reactions of α-terpineol with OH radicals

15   For convenience of description, the atomic number in α-terpineol is labeled in **Scheme 1**.

16   Analysis of the molecular structure of α-terpineol indicates that two types of reaction channels

17   should be considered: (1) addition of OH to the carbon-carbon double bond in the ring and (2)

18   H abstraction from the ring, hydroxyl, and methyl groups, which is supported by Atkinson's

19   experimental work.[41,42] Regarding OH-addition reactions, two reaction pathways, pathways 1

20   and 2, are identified due to the unequivalence of C2 and C3 sites in α-terpineol structure.

21   Depending on the different nature of H atoms in α-terpineol, nine H abstraction reaction

22   processes, pathways 3-11, are taken into consideration in this work. The reaction schemes

1 embedded with the potential barriers ($\triangle E$) and reaction heats ($\triangle H$) are given in **Fig. 1**.

2 Pathways 1 and 2 represent the OH addition to C2 and C3 sites in carbon-carbon double

3 bond, respectively. IM1 (secondary radical) and IM2 (tertiary radical) are the corresponding

4 adducts. Calculation shows that both addition processes are barrierless. The electronic

5 energies of IM1 and IM2 are 26.35 and 28.82 kcal mol^{-1} lower than the total energy of the

6 separate reactants (α-terpineol and OH), respectively. Thus, pathway 1 and 2 can occur readily

7 under the general gas-phase conditions due to their large exoergicity. This provides a

8 theoretical verification for the prior study result.[43] As energy-rich radical intermediates, IM1

9 and IM2 will further react with the oxidizing species, such as O_2 and NO, which are abundant

10 in indoor air environment.

11 As illustrated in **Fig. 1**, pathways 3, 10 and 11 are three kinds of H abstraction from

12 different -CH_3 moieties; pathways 4, 5, 6, 7 and 8 represent four possible hydrogen

13 abstractions from the ring; pathway 9 is H abstraction from the –OH group attached to the C8

14 atom. Comparisons of the nine H abstraction processes show that the abstraction in C5-H7

15 bond, i.e. pathway 6, is the most energetically favorable process. This reaction process can be

16 completed through two elementary steps. The first step is the approaching of OH to the atom

17 H7, which leads to the formation of the pre-complex IM06 with a stabilization energy of -3.02

18 kcal mol^{-1}. Then, the H7 atom is abstracted by OH radical to form IM6 and H_2O via the

19 transition state TS4. The bond lengths of the C5–H7 and O2–H7 in TS4 are 1.166 Å and

20 1.432 Å, respectively. This process has a very low energy barrier of 1.03 kcal mol^{-1}. The

21 energy of IM6 lies 20.07 kcal mol^{-1} below reactants. The same as IM1 and IM2, further

22 reaction of IM6 in indoor air is also ineluctable due to its high reactivity.

3.2. Subsequent reactions

According to the above discussion, both addition and H7 abstraction processes are the dominant pathways for the gas-phase degradation of α-terpineol initiated by OH radicals. Therefore, two additional processes similar to the analogous OH-α-pinene reactions are dominant confirmed in previous experimental and theoretical study.[44,45] In this section, further reactions of the major primary products, IM1, IM2, and IM6, will be discussed in detail.

3.2.1. Subsequent Reaction of IM1

Possible reaction routes from IM1 are presented in **Fig. 2**. The reaction of IM1 with ubiquitous O_2 will proceed via a barrierless association. IM12 is the product with 30.21 kcal mol^{-1} exothermicity. In the presence of nitric oxide, IM12 will react with NO immediately to generate an excited intermediate, denoted as IM13. This process is exoergic by 17.73 kcal mol^{-1}. IM13 has ample internal energy and will subject to prompt isomerization or self-decomposition. The isomerization of IM13 takes place via a three-member ring transition state, TS10, with a potential barrier of 16.44 kcal mol^{-1}. The bond distances of O3-O4 and N-O3 in TS10 are 1.500 Å and 2.277 Å, which are longer by 7.60% and 67.67% than the equilibrium values in reactant adduct and 2-hydroxy-5-(2-hydroxypropan-2-yl)-2-methylcyclohexyl nitrate (P1). The intrinsic reaction coordinate calculation also testifies the synchronism of the fission of O3-O4 and the formation of N-O3. The structure of TS10 is illustrated in **Fig. S2** (see Supplementary material section). The self-decomposition is carried out through the rupture of O3-O4 bond, leading to NO_2 and a radical intermediate, denoted IM14. The transition state of this process is TS11, in which the length of O3-O4 bond is 1.797 Å. This process needs to overcome the

1   barrier of 12.86 kcal mol^{-1}, and release the energy of 3.51 kcal mol^{-1}. Consequently, the

2   self-dissociation reaction of IM13 is more favorable than the isomerization of IM13. IM14 is

3   the preferred product and may play a momentous part in the following reactions of IM1.

4   For IM14, three possible reaction modes are found and described in **Fig. 2**. The first one

5   includes three elementary steps: ring-opening reaction, O_2 addition, and HO_2 elimination. The

6   ring-opening reaction occurs via the cleavage of C2-C3 bond to yield IM15. The energy

7   barrier and endothermic heat are 8.55 and 3.57 kcal mol^{-1}, respectively. Then, O_2 attacks to

8   C2 to generate a peroxide radical (IM16). This process is strongly exothermic by 35.56 kcal

9   mol^{-1}. IM16 is likely to undergo a direct decomposition to form the products

10   3-(2-hydroxypropan-2-yl)-6-oxoheptanal (P2) and HO_2. A five-member ring transition state,

11   TS13, is identified with the barrier of 12.17 kcal mol^{-1}. However, the reaction heat and Gibbs

12   free energy change are 11.81 and 5.53 kcal mol^{-1}, respectively, which indicates that this

13   process is unlikely to occur spontaneously at room temperature. This is in good agreement

14   with the previously reported experimental results.[24] The second channel is initiated from the

15   C3-C4 bond rupture via the transition state TS14. The formation of IM17 is an exoergic

16   process, with the emitting heat of 7.70 kcal mol^{-1} and energy potential barrier of 13.45 kcal

17   mol^{-1}. Similar to IM12, the subsequent reactions of IM17 with O_2/NO also occur via two

18   free-barrier steps to produce IM19. IM19 is not a stable product and will immediately

19   decompose into the oxyl radical IM20 and NO_2, which needs to surmount the barrier height of

20   19.19 kcal mol^{-1}. The following reaction is the direct H abstraction by O_2 molecule via the

21   transition state TS16 with an energy barrier of 17.91 kcal mol^{-1}. The production of

22   2-hydroxy-5-(2-hydroxypropan-2-yl)-2-methylhexanedial (P3) and HO_2 accompanies the

1   exothermic heat of 29.24 kcal mol^{-1}. The third pathway is the reaction of IM14 with O_2,

2   similar   to   the   intermediate   IM20   mentioned   above,   to   produce

3   2-hydroxy-5-(2-hydroxypropan-2-yl)-2-methylcyclohexan-1-one (P4) and HO_2. This reaction

4   process has an apparent barrier of 17.30 kcal mol^{-1}. Through the above analysis, P3 and P4

5   are the possible products from further reaction of IM14.

6   **3.2.2. Subsequent Reaction of IM2**

7   As depicted in **Fig. 3**, the reaction of IM2 with molecular O_2/NO has the similar routes

8   with that of IM1, forming the peroxy intermediate IM22. The same as IM16, the following

9   reaction   of   IM22   also   occurs   via   isomerization   to   produce

10   4-(2-hydroxypropan-2-yl)-1-methylcyclohexane-1,2-diol compound with nitromethane (P5)

11   or unimolecular decomposition to yield IM23 and NO_2. For the two processes, the energy

12   barriers are calculated to be 15.06 and 11.54 kcal mol-1, respectively. Therefore, the

13   decomposition reaction of IM22 is of critical importance in the whole removal process of IM2.

14   As the vital radical intermediate, IM23 has the unpaired electron and can further react through

15   three channels: two ring cleavage reactions and one decomposition reaction.

16   The first one is carried out by the fission of C2-C3 bond in IM23 via the transition state

17   TS20 to generate IM24. This reaction has a low potential barrier of 5.40 kcal mol^{-1} and is

18   exothermic by 2.46 kcal mol^{-1}. IM24 is an open-shell radical and could subsequently react via

19   the reaction with O_2 or the self-decomposition reaction. First, the active site C3 in IM24 is

20   attacked by the oxygen molecule, which is a free-barrier exothermic reaction, to result in

21   IM25. Then, HO_2 is dissociated to form the product 3-(2-hydroxypropan-2-yl)-6-oxoheptanal

22   (P6) via TS21 with the energy barrier of 12.30 kcal mol^{-1}. This decomposition reaction is

1   found to be endothermic with the energy of 12.03 kcal mol^{-1}. Moreover, the Gibbs free energy

2   change is 4.03 kcal mol^{-1}. As a consequence, this decomposition process is difficult to occur

3   spontaneously under normal conditions. Second, the self-decomposition is the breakage of

4   C4-C5 bond to form ethenol (P7) and IM26 via the transition state TS22. In TS22 structure,

5   the length of C4-C5 bond is 2.256 Å, which is elongated by 46.40% with respect to IM24.

6   This process has a potential barrier of 17.34 kcal mol^{-1} and is exothermic by 17.34 kcal mol^{-1}.

7   Two reaction pathways are open for IM26. The first channel is the breaking of C5-C8 bond to

8   form 6-hydroxy-hept-5-en-2-one (P8) and methyl (CH_3). TS23 is the corresponding transition

9   state with the potential barrier of 30.68 kcal mol^{-1}, which means this decomposition reaction

10   is energetically favorable under general condition. The structure of TS23 is shown in **Fig. S2**.

11   The second route is the reaction with O_2/NO through two barrierless associations, to produce

12   IM28. The intermediate IM28 is one energy-rich radical which can react via two serial

13   decomposition processes, resulting in the production of 4-oxopentanal (P9) and IM30 radical.

14   Calculations show that these two elementary reactions can easily occur because of low

15   potential barriers and exothermic property. IM30 is an open-shell radical and will react with

16   O_2 to generate a peroxide intermediate IM31 with 35.25 kcal mol^{-1} exothermicity.

17   Subsequently, H12 migration and C8-O2 bond cleavage occur simultaneously, leading to the

18   final product acetone (P10) and HO_2 radical. This process has an energy barrier of 12.98 kcal

19   mol^{-1} and is believed to proceed easily indoors. According to the description above, P7, P8,

20   and P9 are the preferred products for this removal pathway of IM23.

21   The second channel of IM23 includes four elementary reactions: two barrierless

22   processes (O_2 addition and NO addition) and two elementary processes with apparent

1   potential barriers (cleavage of O4-O5 bond and direct H11 abstraction by O_2). TS28 and TS29

2   are the corresponding transition states and their geometric parameters are given in **Fig. S2**.

3   The calculated results manifest that these elementary steps are energetically favorable under

4   normal   conditions,   which   means   that   the   product   of

5   5-hydroxy-3-(2-hydroxypropan-2-yl)-6-oxoheptanal (P11) should exist in smog chamber.

6   Unfortunately, P11 was not detected in the study of Wells.[24] Further experimental observation

7   would be anticipated to confirm the formation of P11.

8   The third channel is the direct decomposition of IM23 via the rupture of C1-C2 bond to

9   produce   2-hydroxy-4-(2-hydroxypropan-2-yl)cyclohexan-1-one   (P12)   and CH_3.   The

10   calculated profiles of the potential energy surface show that this channel is energetically

11   unfavorable due to the high barrier and strong endothermicity. In other worlds, P12 is not the

12   final product of the OH-initiated gas-phase reaction of α-terpineol.

13   **3.2.3. Subsequent Reaction of IM6**

14   On the basis of the experimental assumption,[23] IM6 can directly decompose into two

15   intermediate radicals IM36 and IM30 via the C5-C8 bond breakage. And then, P14 can be

16   formed from IM136 via a series of elementary steps. However, our calculated results indicate

17   that this decomposition process is barrierless but stongly endothermic by 82.96 kcal mol^{-1}.

18   Besides, the Gibbs free energy change is 70.07 kcal mol^{-1}, which is far greater than zero.

19   Therefore, we can infer that the decomposition reaction of IM6 can hardly occur. To wit: this

20   proposed reaction pathway of IM6 to form P14 is unreasonable under the general condition.

21   Another possible removal pathway of IM6 was revealed in this study. The detailed

22   reaction scheme for this reaction pathway of IM6 is shown in **Fig. 4**. IM6 may react easily

1   with O_2 and NO, in turn, via two exothermic processes to generate IM38. The structure of

2   IM38 is shown in **Fig. S3**, which is similar to IM13 and IM22. Also, two possible reaction

3   routes are considered. One route is the formation of P13 via the isomerization of IM38, which

4   has a potential barrier of 16.89 kcal mol^{-1} and is highly exothermic by 29.15 kcal mol^{-1}. The

5   other route is the formation of P14 that involves two self-decomposition reactions.

6   Calculations show that both decomposition processes are energetically favorable due to low

7   potential barriers. Unluckily, this formation pathway of P14 was not considered in Jones'

8   study. [23] This energetically favorable formation pathway of P14 is reported for the first time

9   and its confirmation needs further more experimental investigations.

10 **3.3. Rate constants calculations**

11   According to the data calculated by Gaussian09, the kinetic calculations are performed

12 using the RRKM method. The rate constants of the elementary reactions involved in this

13 reaction system were calculated at 298 K and 1 atm. The computational results are presented

14 in T**able 1,** and after the errors were considered, the rate constants at 298 K are listed in **Table**

15 **S1**. The overall rate constant of α-terpineol + OH (**Table 1**) is 1.29×10^{-10} cm^3 molecule^{-1} s^{-1},

16 which is in keeping with the experimental value of 1.9×10^{-10} cm^3 molecule^{-1} s^{-1} at 298 K and

17 1 atm total pressure. It could be deduced that our RRKM results listed in **Table 1** are

18 reasonable. With the comparison of individual rate coefficients, OH addition to C2 and C3

19 atoms and H abstraction from C5 atom, i.e. the formation of IM1, IM2 and IM6, are the

20 dominant pathways. This conclusion accords well with the thermodynamic data in section 3.1.

21 The kinetical data mentioned above would be conductive to the construction of dynamic

22 model predicting the transport and fate of α-terpineol and OH radical in indoor air.

1   The residence time of α-terpineol in indoor air can be calculated by the formula

2    $\tau = \dfrac{1}{k[OH]}$. Here, k is the total rate constant of the title reaction and [OH] is the average indoor

3   OH concentration with the value about 7×10^5 molecule cm^{-3}.[46] The gas phase retention time

4   of α-terpineol determined by OH radicals is approximately 3.1 hours at 298 K and 1 atm total

5   pressure.

6   **4. Conclusions**

7   In this paper, the gas-phase oxidation mechanism of α-terpineol initiated by OH radical

8   was investigated by using a high-accuracy quantum chemical method. All of the rate constants

9   were calculated using the MESMER program. The following conclusions can be obtained

10   based on the theoretical calculations:

11   (1)There are two possible reaction mechanisms (OH additions and H abstractions) during

12   the reaction between α-terpineol and OH radical. According to different chemical

13   environments, two sites for OH addition and nine distinct sites for hydrogen abstraction are

14   identified. Among the primary reactions, two free-barrier addition processes and the

15   H7-abstraction from the ring are the main reaction pathways.

16   (2)   Based   on   our   calculation   results,

17   2-hydroxy-5-(2-hydroxypropan-2-yl)-2-methylhexane-dial   (P3),

18   2-hydroxy-5-(2-hydroxypropan-2-yl)-2-methylcyclohexan-1-one   (P4),

19   6-hydroxy-hept-5-en-2-one (P8) , 4-oxopentanal (P9), and acetone (P10) are the energetically

20   feasible products from the pathways of OH addition to the >C=C< bond.

21   4-methyl-3-cyclohexen-1-one (P14) is the possible product of the most favorable

22   H-abstraction pathway. The suggested formation mechanism of P14 in the study of Jones is

1 unreasonable. An energetically favorable formation pathway for P14 is reported for the first

2 time.

3 (3) The rate constant calculations show that OH radicals are preferred to react with

4 α-terpineol through addition reaction at 298 K and 1 atm. The total rate constant of the title

5 reaction is 1.29×10^{-10} cm^3 molecule^{-1} s^{-1}, which matches well with the available experimental

6 values. The gas-phase residential time of α-terpineol with the respect of OH is about 3.1

7 hours.

8

9

15

16

17

18

19

20

21

22

References

1   H. Guo, S. C. Lee, L. Y. Chan and W. M. Li, *Environ. Res.*, 2004, **94**, 57-66.

2   C. J. Weschler, *Sci. World. J.*, 2001, **1**, 443-457.

3   C. J. Weschler and H. C. Shields, *Atmos. Environ.*, 1997a, **31**, 3487-3495.

4   M. Maroni, B. Seifert and T. Lindvall (Eds.), I*ndoor Air quality-a comprehensive reference book*, Elsevier Publishers, Amsterdam, 1995.

5   D. Otto, H. Hudnell, D. House, L. Molhave and W. Counts, *Arch. Environ. Health*, 1992, **47**, 23-30.

6   B. T. Burton, *Volatile organic compounds*, Dekker, New York, 1997.

7   M. J. Hodgson, J. Frohlinger, E. Permar, C., Tidwell, N. D. Traven, S.A. Olenchock and M. Karpf, *J. Occup. Med.*, 1991, **33**, 527-533.

8   L. Molhave, *Indoor Air*, 1991, **1**, 357-376.

9   L. Molhave, G. Clausen, B. Berglund, J. D. Ceaurriz, A. Kettrup, T. Lindvall, M. Maroni, A. C. Pickering, U. Risse, H. Rothweiler, B. Seifert and M. Younes, *Indoor Air*, 1997, **7**, 225-240.

10   L. Molhave, J. G. Jensen and S. Larsen, *Atmos. Environ.* 1991, **25A**, 1283-1293.

11   E. Ota and E. Mulberg, *Exposure to formaldehyde from indoor air*, California Air Resources Board, Technical Report ARB/RD-90-01, 1990.

12   J. C. Harrison and J. E., Ham, *Int. J. Chem. Kinet.*, 2010, **42**, 669-675,

13   A. Lapczynski, C. S. Letizia and A. M. Api, *Food Chem. Toxicol.*, 2008, **46**, S126-S127.

14   A. Lapczynski, C. S. Letizia and A. M. Api, *Food Chem. Toxicol.*, 2008, **46**, S114-S116.

15   V. T. Politano, E. M. Lewis, A. M. Hoberman, M. S. Christian, R. M. Diener and A. M.

1 Api, *Int. J. Toxicol.*, 2009, **28**, 80-87.

2 16 W. W. Nazaroff and C. J. Weschler, *Atmos. Environ.*, 2004, **38**, 2841-2865.

3 17 J. M. Logue, T. E. Mckone, M. H. Sherman and B. C. Singer, *Indoor Air*, 2011, **21**,

4 92-109.

5 18 B. C. Singer, H. Destaillats, A. T. Hodgson and W. W. Nazaroff, *Indoor Air*, 2006,**16**,

6 179-191.

7 19 B. Wessen and K. O. Schoeps, *Analyst*, 1996, **121**, 1203-1205.

8 20 P. Gao and J. Martin, *Appl. Occup. Environ. Hyg.*, 2002a,**17**, 430-436.

9 21 P. Gao, F. Korley, J. Martin and B. T. Chen, *J. Am. Ind. Hyg. Assoc.*, 2002b, **63**, 135-140.

10 22 M. S. Waring and J. R. Wells, *Atmos. Environ.*, 2015,**106**, 382-391.

11 23 B. T. Jones and J. E. Ham, *Atmos. Environ.*, 2008, **42**, 6689-6698.

12 24 J. R. Wells, *Environ. Sci. Technol.*, 2005, **39**, 6937-6943.

13 25 Q. Zhang, X. Qu, H. Wang, F. Xu, X. Shi and W. Wang, *Environ. Sci. Technol.*, 2009, **43**,

14 4105-4112.

15 26 L. Tadeu, B. Leonardo, C. S. Edilson and A. Graciela, *J. Phys. Chem. A*, 2011, **115**,

16 7709-7721.

17 27 X., Sun, C. Zhang, Y. Zhao, J. Bai, Q. Zhang and W. Wang, *Environ. Sci. Technol.*, 2012,

18 **46**, 8148-8155

19 28 X. Sun, J. Bai, Y. Zhao, C. Zhang, Y. Wang and J. Hu, *Atmos. Environ.*, 2011, **45**,

20 6197-6203

21 29 M. S. Waring and J. R. Wells, *Atmos. Environ.*, 2015, **106**, 382-391.

22 30 M. Frisch, G. Trucks, H. B. Schlegel, G. Scuseria, M. Robb, J. Cheeseman, G. Scalmani,

1 V. Barone, B. Mennucci and G. Petersson, 2009. Gaussian 09, revision A. 02; Gaussian.

2 Inc., Wallingford, CT 270, 271.

3 31 Y. Zhao and D. G. Truhlar, *J. Phys. Chem. A*, 2004, **108**, 6908-6918.

4 32 Y. Zhao, B. J. Lynch and D. G. Truhlar, *J. Phys. Chem. A*, 2004, **108**, 2715-2719.

5 33 J. J. Zheng, Y. Zhao and D. G. Truhlar, *J. Chem. Theory Comput.*, 2009, **5**, 808-821.

6 34 C. Gonzalez and H. B. Schlegel, *J. Phys. Chem.*, 1990, **94**, 5523-5527.

7 35 P. J. Robinson and K. A. Holbrook, *Unimolecular Reactions*, Wiley, New York, 1972.

8 36 S. H. Robertson, D. R. Glowacki, C. H. Liang, C. Morley and M. J. Pilling, *MESMER*

9 *(Master Equation Solver for Multi-Energy Well Reactions)*, *an object oriented C++*

10 *program for carrying out ME calculations and eigenvalue-eigenvector analysis on*

11 *arbitrary multiple well systems*, Available from: http://sourceforge.net/projects/mesmer,

12 2008.

13 37 J. Zhou, J. W. Chen, C. H. Liang, Q. Xie, Y. N. Wang, S. Y. Zhang, X. L. Qiao and X. H.

14 Li, *Environ. Sci. Technol.*, 2011, **45**, 4839-4845.

15 38 D. R. Glowacki, C. H. Liang, C. Morley, M. J. Pilling and S. H. Robertson, *J. Phys.*

16 *Chem. A*, 2012, **116**, 9545-9560.

17 39 S. Coussan, Y. Bouteiller and J. P. Perchard, *J. Phys. Chem. A*, 1998, **10**2, 5789-5793.

18 40 CCCBDB (Computational Chemistry Comparison and Benchmark Database), Available

19 from: http://cccbdb.nist.gov/, 2015.

20 41 R. Atkinson, *Kinetics and mechanisms of the gas-phase reactions of the hydroxyl radical*

21 *with organic compounds*, J. Phys. Chem. Ref. Dat. Monograph 1, 1989.

22 42 R. Atkinson, *Gas-phase tropospheric chemistry of organic compounds*, J. Phys. Chem.

23 Ref. Dat. Monograph 2, 1994.

1   43 R. S. Boethling and D. Mackay, *Handbook of property estimation methods for chemicals:*

2   *environmental and health sciences*, Lewis Publishers, New York, 2000.

3   44 M. E. Davis and P. S. Stevens, *Atmos. Environ.*, 2005, **39**, 1765-1774.

4   45 L. Vereecken and J. Peeters, *J. Phys. Chem. A*, 2000, **104**, 11140-11146.

5   46 G. Sarwar, R. Corsi, Y. Kimura, D. Allen and C. J. Weschler, *Atmos. Environ.*, 2002, **36**,

6   3973-3988.

7

8

9

10

11

12

13

14

15

1   **Figure, Scheme and Table Captions**

2   **Scheme 1** The atomic number of α-terpineol.

3   **Fig. 1** The primary reaction pathways of α-terpineol with OH radical embedded with the

4   potential barriers ΔE (kcal mol^{-1}) and reaction heats ΔH (kcal mol^{-1}) at the

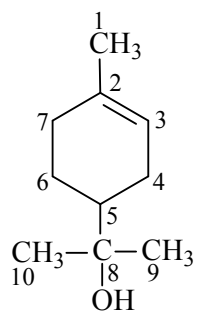5   MPWB1K/6-31+G(d,p)// MPWB1K/6-311+G(3df,2p) level.

6   **Fig. 2** Subsequent reaction paths of IM1 at the MPWB1K/6-31+G(d,p) level of theory. Unit:

7   kcal mol^{-1}. ΔE: the reaction potential barrier; ΔH: the reaction heat.

8   **Fig. 3** Subsequent reaction paths of IM2 at the MPWB1K/6-31+G(d,p) level of theory. Unit:

9   kcal mol^{-1}. ΔE: the reaction potential barrier; ΔH: the reaction heat.

10   **Fig. 4** Subsequent reaction paths of IM6 at the MPWB1K/6-31+G(d,p) level of theory. Unit:

11   kcal mol^{-1}. ΔE: the reaction potential barrier; ΔH: the reaction heat.

12   **Table 1** The rate constants (cm^3 molecule^{-1} s^{-1} or s^{-1}) of the elementary reactions involved in

13   the gas-phase oxidation of α-terpineol with OH radicals at 298 K and 1 atm.

14

$$\underset{1}{CH_3}$$

(Chemical structure: cyclohexene ring with positions labeled 2 (top, bearing CH₃ group 1), 3 (upper right), 4 (lower right), 5 (bottom, bearing C(OH)(CH₃)₂ group), 6 (lower left), 7 (upper left); double bond between positions 2 and 3. The substituent at position 5 is $CH_3-\underset{\underset{OH}{|8}}{C}-CH_3$ with the CH₃ groups labeled 10 and 9.)

Scheme 1

Fig.1

2

Fig.2

3

Fig.3

4

Fig.4

5

Table 1 The rate constants (cm^3 molecule^{-1} s^{-1} or s^{-1}) of the elementary reactions involved in the gas-phase oxidation of α-terpineol with OH radicals at 298 K and 1 atm.
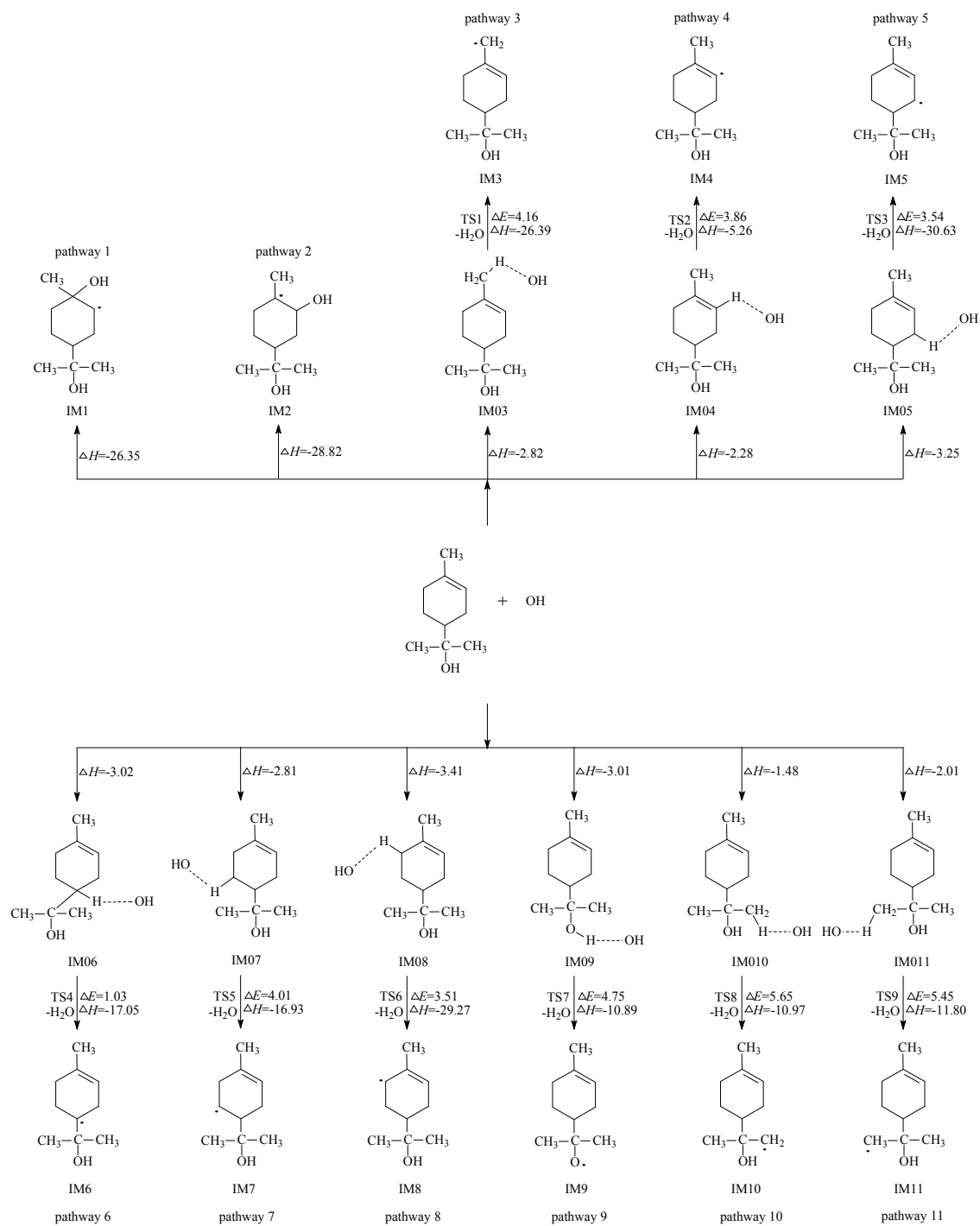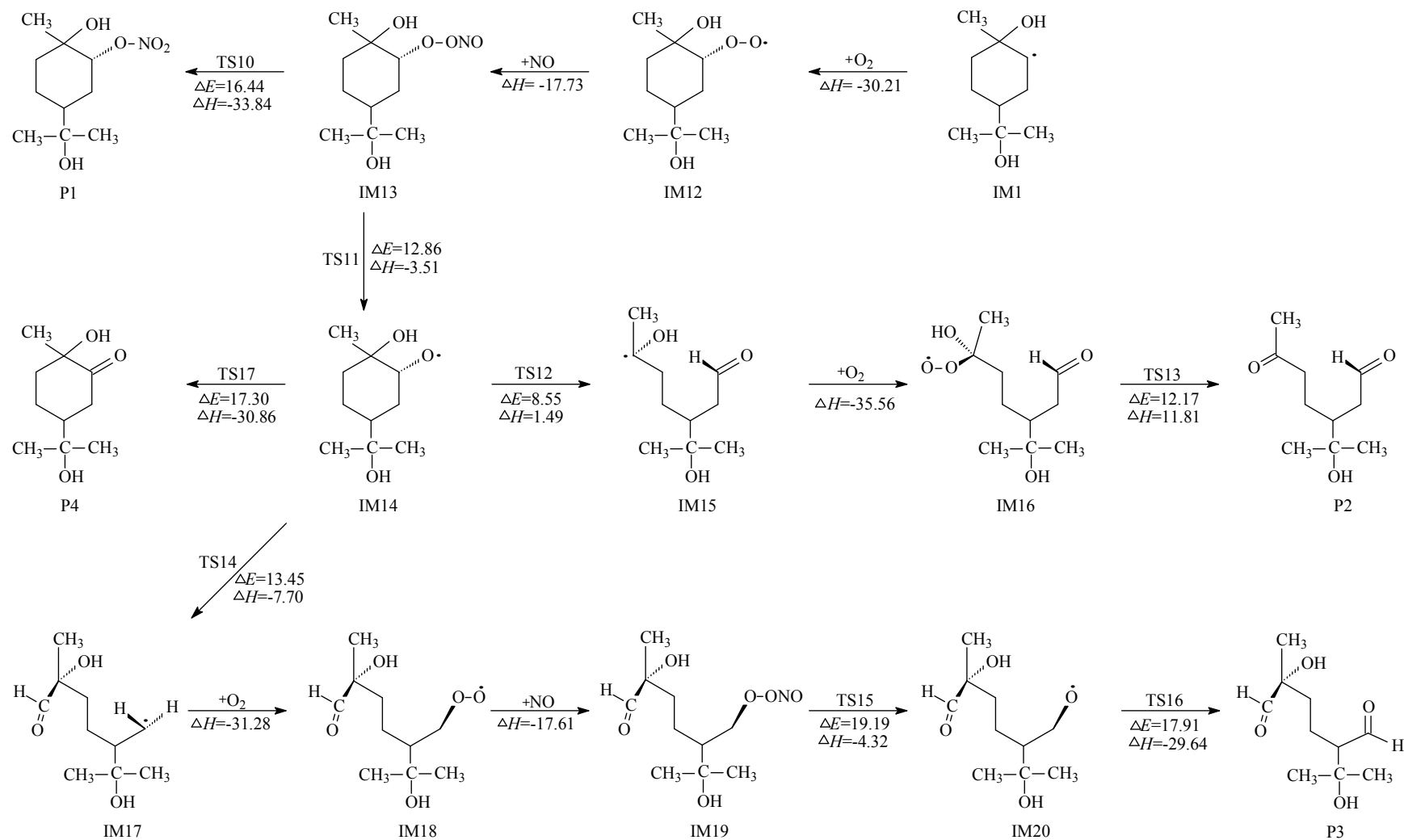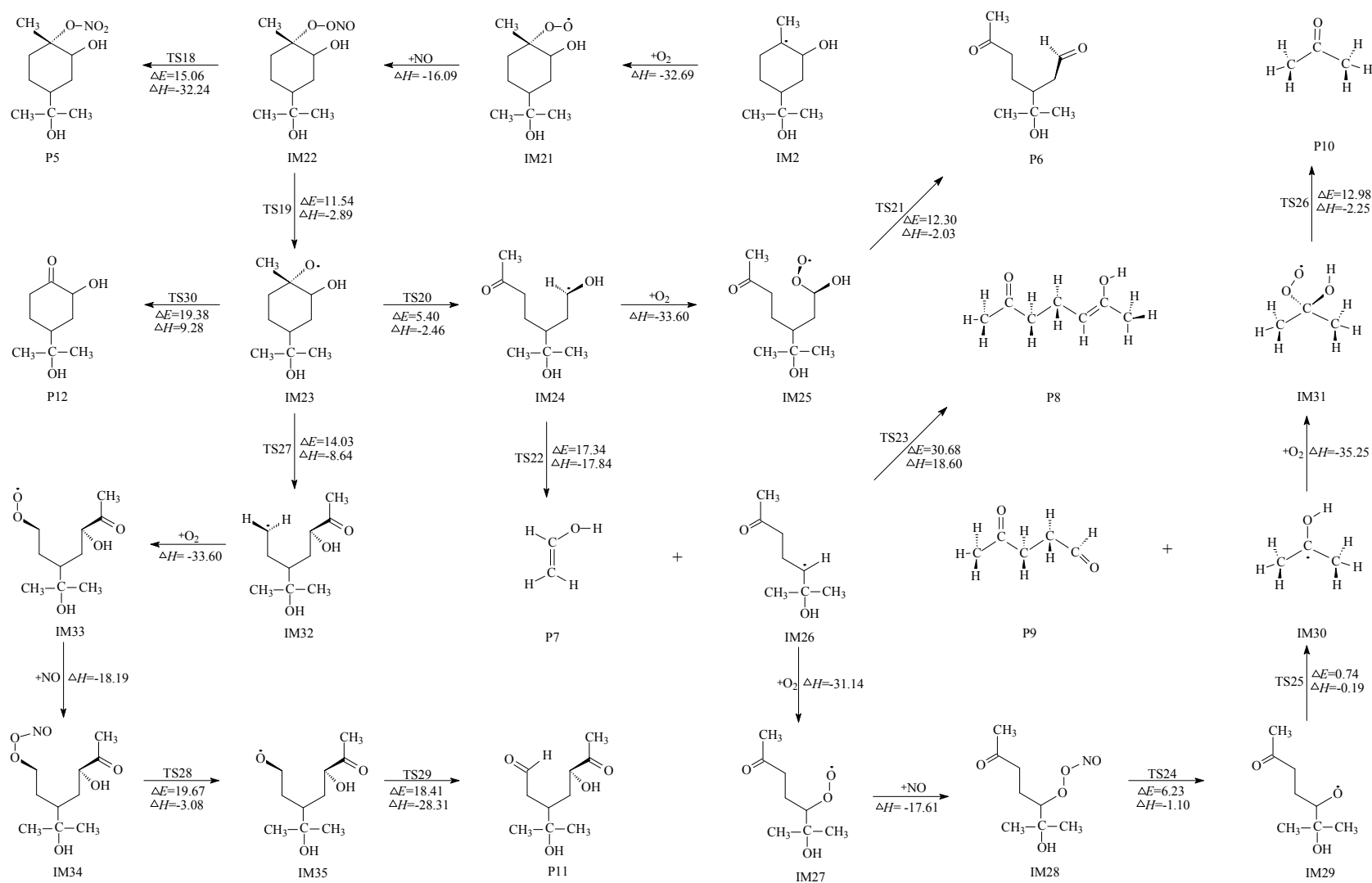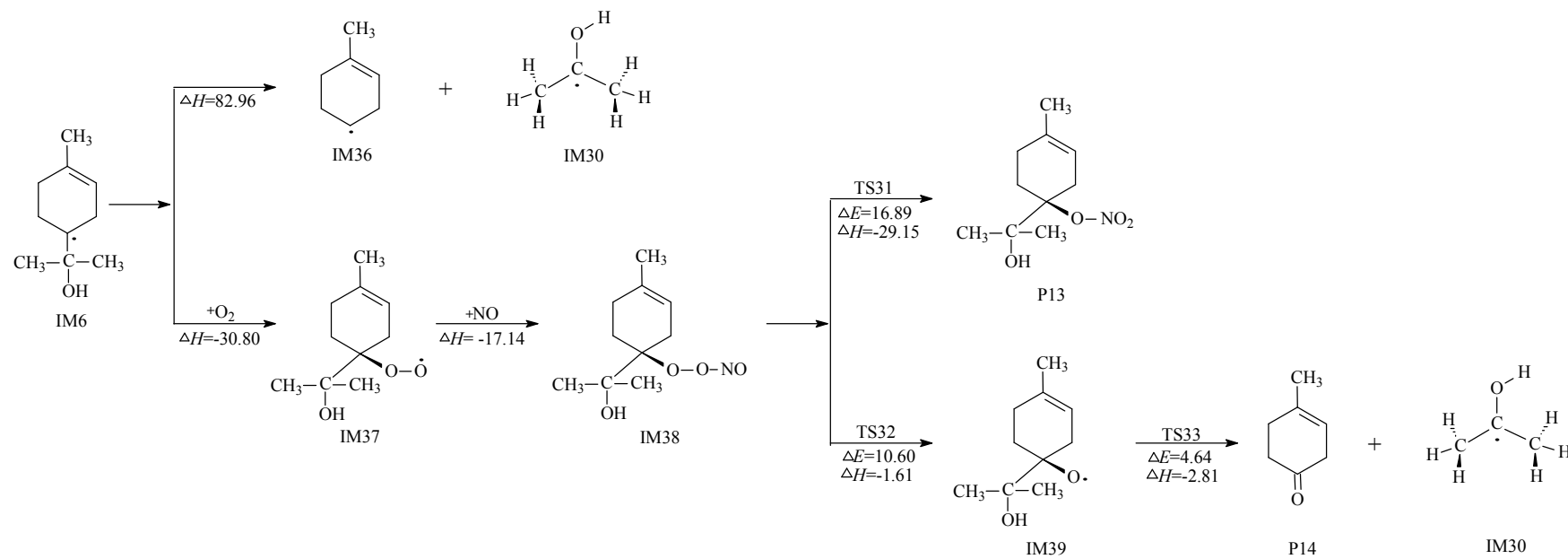
Reactions	Rate constants	Reactions	Rate constants
R+OH→IM1	5.95×10^{-11}	IM21+NO→IM22	4.36×10^{-12}
R+OH→IM2	6.37×10^{-11}	IM22→P5	4.78×10
R+OH→IM3+H$_2$O	2.10×10^{-13}	IM22→IM23+NO$_2$	5.17×10^{4}
R+OH→IM4+H$_2$O	1.31×10^{-14}	IM23→IM24	2.66×10^{7}
R+OH→IM5+H$_2$O	7.04×10^{-13}	IM24+O$_2$→IM25	5.40×10^{-12}
R+OH→IM6+H$_2$O	3.64×10^{-12}	IM25→P6+HO$_2$	1.41×10^{4}
R+OH→IM7+H$_2$O	1.96×10^{-14}	IM24→IM26	2.85×10^{-8}
R+OH→IM8+H$_2$O	7.19×10^{-13}	IM26→P8+CH$_3$	4.52×10^{-10}
R+OH→IM9+H$_2$O	1.73×10^{-15}	IM26+O$_2$→IM27	5.90×10^{-12}
R+OH→IM10+H$_2$O	1.27×10^{-15}	IM27+NO→IM28	6.21×10^{-12}
R+OH→IM11+H$_2$O	1.37×10^{-13}	IM28→IM29+NO$_2$	2.96×10^{7}
R+OH	(k)1.29×10^{-10}	IM29→IM30+P9	2.43×10^{9}
IM1+O$_2$→IM12	5.78×10^{-12}	IM30+O$_2$→IM31	6.01×10^{-12}
IM12+NO→IM13	7.11×10^{-12}	IM31→P10+HO$_2$	2.31×10^{3}
IM13→P1	1.06	IM23→IM32	4.32×10
IM13→IM14+NO$_2$	2.22×10^{3}	IM32+O$_2$→IM33	5.35×10^{-12}
IM14→IM15	3.46×10^{6}	IM33+NO→IM34	6.45×10^{-12}
IM15+O$_2$→IM16	5.43×10^{-12}	IM34→IM35+NO$_2$	0.12
IM16→P2+HO$_2$	9.80×10^{3}	IM35+O$_2$→P11+HO$_2$	5.71×10^{-53}
IM14→IM17	1.52×10^{3}	IM23→P12+CH$_3$	1.09×10^{-2}
IM17+O$_2$→IM18	5.28×10^{-12}	IM6+O$_2$→IM37	5.96×10^{-12}
IM18+NO→IM19	5.83×10^{12}	IM37+NO→IM38	6.10×10^{-12}
IM19→IM20+NO$_2$	0.10	IM38→P13	1.08
IM20+O$_2$→P3+HO$_2$	7.20×10^{-53}	IM38→IM39+NO$_2$	7.18×10^{4}
IM14+O$_2$→P4+HO$_2$	4.50×10^{-27}	IM39→IM30+P14	1.68×10^{8}
IM2+O$_2$→IM21	5.78×10^{-12}		

6
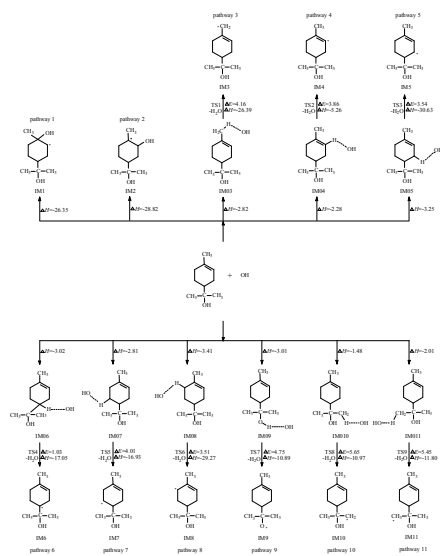
For the OH-initiated indoor oxidation of *α*-terpineol, the reaction scheme is proposed and the main reaction pathways are reported.